

# Effects of equation of state on hydrodynamic expansion, spectra and flow harmonics

Danuce M. Dudek<sup>1</sup>, Wei-Liang Qian<sup>2</sup>, Chen Wu<sup>3</sup>, Otávio Socolowski Jr.<sup>4</sup>,  
Sandra S. Padula<sup>1</sup>, Gastão Krein<sup>1</sup>, Yojiro Hama<sup>5</sup>, Takeshi Kodama<sup>6</sup>

<sup>1</sup>*Instituto de Física Teórica, Universidade Estadual Paulista,*

*Rua Dr. Bento Teobaldo Ferraz, 271 - Bloco II, 01140-070 São Paulo, SP, Brazil*

<sup>2</sup>*Escola de Engenharia de Lorena, Universidade de São Paulo, 12602-810, Lorena, SP, Brazil*

<sup>3</sup>*Shanghai Institute of Applied Physics, Shanghai 201800, China*

<sup>4</sup>*Instituto de Matemática Estatística e Física, Universidade Federal do Rio Grande,*  
*Caixa Postal 474, 96201-900 Rio Grande, RS, Brazil*

<sup>5</sup>*Instituto de Física, Universidade de São Paulo,*

*Caixa Postal 66318, 05389-970 São Paulo, SP, Brazil and*

<sup>6</sup>*Instituto de Física, Universidade Federal do Rio de Janeiro,*

*Caixa Postal 68528, 21941-972 Rio de Janeiro, RJ, Brazil*

(Dated: Aug. 29, 2014)

We perform a systematic study of the role played by the equation of state in the hydrodynamic evolution of the matter produced in relativistic heavy ion collisions. By using the same initial conditions and freeze-out scenario, the effects of different equations of state are compared by calculating their respective hydrodynamical evolution, particle spectra and elliptic flow parameter  $v_2$ . Three different types of equation of state are studied, each focusing on different features, such as the nature of the phase transition, as well as strangeness and baryon densities. Different equations of state imply different hydrodynamic responses, the impact thereof on final state anisotropies are investigated. The results of our calculations are compared to the data of two RHIC energies, 130 GeV and 200 GeV. It is found that the three equations of state used in the calculations describe the data reasonably well; differences can be observed, but they are quite small. The insensitivity to the equation of state weakens the need for a locally thermalized description of the system, at least for the observables analysed in the present work.

## I. INTRODUCTION

The equation of state (EoS) of strongly interacting matter plays a major role in the hydrodynamic description of the hot and dense matter created in heavy ion collisions [1–4]. It governs how the hydrodynamic evolution transforms the initial state fluctuations into final state anisotropies in terms of collective flow and particle correlations. Motivated by the lattice QCD simulations which indicate that the quark-hadron transition is a crossover at zero baryon density [5–7], many different equations of state (EoSs) have been proposed by fitting the lattice data [8, 9], complemented by combining with EoSs appropriate for the hadronic phase [10] at low temperatures [11–19]. For a study employing EoS with a first order phase transition, see Ref. [20].

The assumption of zero baryon density is a fairly good approximation for the initial conditions (IC) of the systems created at RHIC and LHC, but strongly interacting matter possesses several conserved charges such as electric charge, net baryon number and strangeness. Studies have shown [21–23] that the thermodynamic properties as well as phase transitions are modified when the number of degrees of freedom of the system changes. In the case of a liquid-gas phase transition, for instance, the increase of the number of degrees of freedom increases the dimension of the binodal surface and the corresponding transition is continuous rather than discontinuous [24–26]. In view of this, one can expect that in the case of the QCD matter the conserved charges may affect the duration of the hydrodynamic evolution of the system in the

transition region and would likely manifest themselves at the stage of hadronization. Therefore, experimental data on multiplicity, ratio of particle yields and their fluctuations need to be analysed through models properly handling finite baryon density and strangeness. A statistical model with finite chemical potential is capable of describing the data reasonably well [27–30], which indicates that it might be essential for the study of the evolution of the system to use EoSs that provide reasonable description of the matter produced over a large range of densities and temperatures. Following this line of thought, a compromise was proposed by Hama et al. [31], where a phenomenological critical point is introduced to smoothen the transition region where the baryon density is smaller than that of the critical point. In the model, finite baryon chemical potential is taken into consideration in both the Quark-Gluon Plasma (QGP) and in the hadronic phase. Such an approach reflects well the main characteristic of a smooth crossover transition while explicitly considering non-zero baryon density. Unfortunately, in the QGP phase, the model does not accurately reproduce asymptotic properties of the QGP matter.

The present work employs different EoSs in an ideal hydrodynamical model to study their effects on particle spectra and flow harmonics. In the following section, we briefly review different EoSs employed in the literature and then discuss those EoSs employed in the present work. In section III we present the results of our hydrodynamical simulations. We compute particle spectra and the elliptic flow parameter  $v_2$  of charged particles as well as of identified particles. The calculations are done for

RHIC energies of 130 GeV and 200 GeV, and for various different centrality windows. Conclusions and perspectives for future work are presented in section IV.

## II. EQUATION OF STATE AND HYDRODYNAMICAL MODEL

Many different EoSs compatible with results of lattice QCD simulations have been investigated in the literature. Huovinen [11] proposed an EoS connecting a lattice QCD EoS to another one for a hadronic resonance gas (HRG) model, and requiring continuity of the entropy density and its derivatives in the transition region, where no data is available. In a later work, Huovinen and Petreczky [12] improved the parameterization of Ref. [11] by focusing on the trace anomaly,  $\Theta \equiv T^\mu{}_\mu = e - 3P$ : the EoS adopts the lattice EoS at high temperature and connects it smoothly to an EoS of a HRG model at low temperature by requiring that the trace anomaly as well as its first and second derivatives to be continuous. Since then the EoS has been adopted in many studies. In Refs. [14, 32], an EoS was proposed also based on the lattice data and a HRG model. In this EoS, the sound velocity was interpolated in the transition region and by means of thermodynamical relations, the sound velocity is constrained to match the lattice QCD entropy density by an integral in temperature. A few other EoSs were proposed in a similar fashion [15, 16, 18], using a lattice EoS at high temperatures and connecting it to a phenomenological hadronic EoS using different prescriptions. In some of those, there are issues of thermodynamic consistency.

On the other hand, instead of interpolating lattice QCD data, some works focused on EoSs with a critical end point in the phase diagram. In Ref. [31], for instance, a phenomenological critical point is introduced via an EoS from the MIT bag model for the QGP phase, connected to an EoS of a HRG model for the hadronic phase. Another attempt was implemented in Ref. [33], where an SU(3) Polyakov-Nambu-Jona-Lasinio (PNJL) model was used for the high temperature phase. A critical end point is naturally obtained by using the Polyakov loop as the order parameter of the deconfinement transition.

We note that most of the EoSs discussed above consider only zero baryon density. Moreover, in the hydrodynamical simulations, usually averaged IC were used, and only a few works previously adopted full three-dimensional (3-D) hydrodynamical simulations. Though it was estimated in Refs. [11, 34] that the effect of finite chemical potential is small, less than a few percent, it is not clear, whether its importance may increase for event-by-event IC. In addition, in most studies, calculations were only done for some specific collision energy and centrality windows. In view of these, it seems worthwhile to carry out an event-by-event 3-D simulation on the effects of the equation of state, covering a broader range of the published data.

In this work, hydrodynamical calculations are carried

out by using the full 3-D ideal hydrodynamical code NEXSPheRIO. For more realistic collisions, the effect of viscosity should be taken into account. However, the main purpose of this study is to investigate the difference between various EoSs rather than to reproduce the data precisely, and viscosity usually reduces such differences. Besides, viscosity may also introduce extra theoretical uncertainties, such as viscous correction from equilibrium distribution on the freeze-out surface [35, 36]. The NEXSPheRIO code uses IC provided by the event generator NeXuS [37, 38] and solves the 3+1 ideal hydrodynamic equations with the SPheRIO code [20, 39]. By generating many NeXuS events, and solving independently the equations of hydrodynamics for each of them, one takes into account the fluctuations of IC on an event-by-event basis. At the end of the hydrodynamic evolution of each event, a Monte-Carlo generator is employed to produce hadrons following a Cooper-Frye prescription, and then the hadronic decay is considered. A limited list of references describing studies of heavy-ion collisions using the NEXSPheRIO code can be found in Refs. [40–46].

In this work, we investigate three different types of EoS:

- (LQCD) A lattice QCD EoS proposed by Huovinen [11] with zero baryon chemical potential,
- (CEP) A lattice QCD inspired EoS [31] with smooth transition and a critical end point, which considers finite baryon chemical potential,
- (FOS) An EoS with first-order phase transition [47] which considers both finite baryon chemical potential and local strangeness neutrality.

The first type of EoS, LQCD, adopts a parameterization of the lattice QCD data for the high temperature region, while assumes a HRG model for the low temperature region. The EoS only considers zero baryon density. In the calculations, the pressure and energy density are obtained through the trace anomaly  $\Theta$  by the following relations [12]

$$\frac{p(T)}{T^4} - \frac{p(T_{low})}{T_{low}^4} = \int_{T_{low}}^T \frac{dT'}{T'^5} \Theta, \quad \varepsilon = \Theta + 3p \quad (1)$$

where a sufficiently small lower limit of integration,  $t_{low}$ , is used in practice.

The second EoS, CEP, considers the following phenomenological parametrization instead of Gibbs conditions for the phase transition

$$(p - p^Q)(p - p^H) = \delta, \quad (2)$$

where  $p^Q$  and  $p^H$  are the pressure in the hadronic and in the QGP phase, respectively;  $\delta = \delta(\mu_b)$  is a function of baryon chemical potential  $\mu_b$  which approaches zero

when  $\mu_b$  is larger than a critical value  $\mu_c$ . Eq.(2) has the following solution

$$p = \lambda p^H + (1 - \lambda)p^Q + \frac{2\delta}{\sqrt{(p^Q - p^H)^2 + 4\delta}}, \quad (3)$$

where

$$\lambda \equiv \frac{1}{2} \left[ 1 + (p^Q - p^H) / \sqrt{(p^Q - p^H)^2 + 4\delta} \right]. \quad (4)$$

It is straightforward to verify that, for small  $\delta$ ,  $p \rightarrow p^Q$  when  $p^Q < p^H$  and  $p \rightarrow p^H$  when  $p^Q > p^H$ . It naturally recovers the first order phase transition when  $\delta = 0$  [31]. The values of  $p^Q$  and  $p^H$  are those determined in an EoS with first-order phase transition (FO) [31] which considers finite baryon chemical potential, and assumes an ideal gas model of quarks and gluons for the QGP phase, as well as a HRG model for hadronic phase. Note that in both CEP and FO, finite baryon density is considered.

The third EoS, FOS, introduces an additional constraint in FO, namely, strangeness neutrality, i.e.

$$\rho_s = 0. \quad (5)$$

The strangeness chemical potential,  $\mu_s$ , is introduced in the EoS as a new variable. Therefore the strangeness chemical potential is not an independent degree of freedom in the system, it merely increases the dimension of the binodal surface of the phase transition [21]. It also modifies the phase structure, as discussed below. Before carrying out the hydrodynamical simulations we first discuss qualitatively the differences among the different EoSs.

We show in Fig. 1 the phase boundaries of the different EoSs. For LQCD, the deconfinement transition corresponds to the parameterization in the region of  $170 \text{ MeV} < T < 220 \text{ MeV}$  on the temperature axis in the plot. For FO and FOS, the phase boundary is determined by the Gibbs conditions between the quark-gluon and hadronic phases. The phase boundary of the CEP is not shown explicitly in the plot, it is almost the same as that of FO beyond the critical point, and is smoothed out below that point. The top plot shows the phase boundaries in terms of temperature as a function of baryon density, while the plot in the bottom shows those in terms of the temperature as a function of baryon chemical potential.

We note that FOS possesses an unique feature: the QGP phase boundary and the hadronic phase boundary have different baryon chemical potentials. It can be seen as a result of the strangeness local neutrality condition. This implies that during the phase transition, when the two phases are in equilibrium, it is not necessary that both phases simultaneously have vanishing strangeness density. This is because in the transition region, the strangeness neutrality condition Eq.(5) reads,

$$\rho_s = \lambda \rho_s^H + (1 - \lambda) \rho_s^Q = 0. \quad (6)$$

In other words, in the case of FOS, neither the strangeness density of hadronic phase ( $\rho_s^H$ ) nor that of

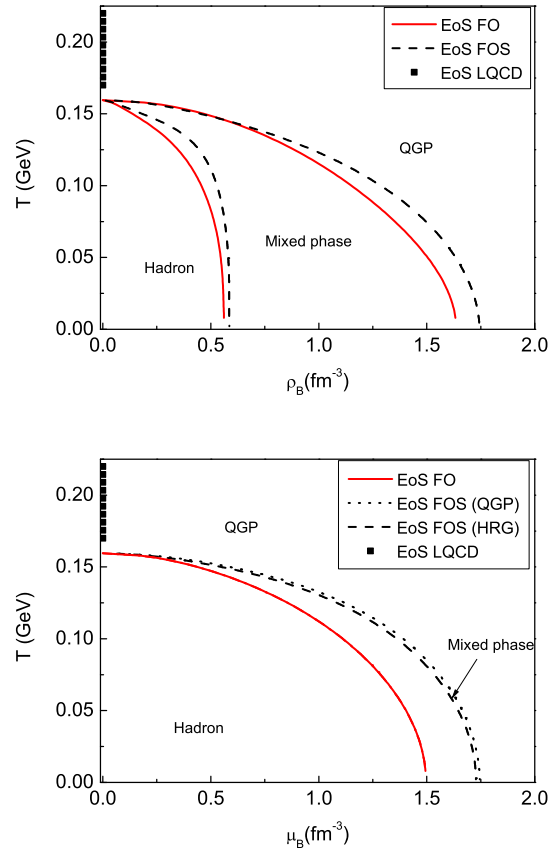


FIG. 1. (Color online) Phase boundaries shown in temperature vs. baryon density (top panel) and in vs. baryon chemical potential (lower panel).

the QGP phase ( $\rho_s^Q$ ) is necessarily zero. Therefore, the baryon chemical potential is not fixed during the phase transition, its value being dependent on the fraction of hadronic phase ( $\lambda$ ) of the system which is in chemical and thermal equilibrium. In general, the resulting baryon chemical potential attains different values on the hadronic phase boundary ( $\lambda = 0$ ) and on the QGP phase boundary ( $\lambda = 1$ ) without violating the Gibbs conditions. As a comparison, in the case of FO, the QGP phase boundary coincides with that of the hadronic phase.

In Fig. 2, we show the pressure as a function of baryon chemical potential, as well as baryon density at a given temperature  $T = 150 \text{ MeV}$  for different EoS. It is worth noting here that for FOS, neither the baryon chemical potential nor the strangeness chemical potential is fixed during the isothermal phase transition procedure. As a result, when expressed in pressure and chemical potential, the transition region of FO is a point, but it is a curve in the case of FOS, as shown in the top plot of Fig.2. When expressed in terms of pressure and baryon density, the transition region corresponds to the horizontal line of constant pressure in the case of FO. On

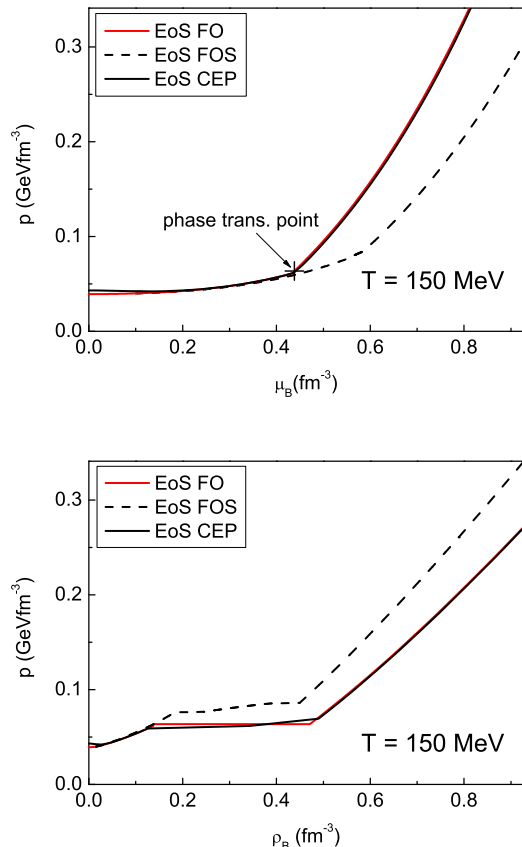


FIG. 2. (Color online) Pressure as a function of baryon chemical potential (top panel) and baryon density (lower panel) at given temperature  $T = 150$  MeV for EoSs CEP, FO, and FOS.

the other hand, the pressure increases during the phase transition in the case of FOS. Therefore, the phase transition in FOS is smoother than that in FO. For the CEP EoS, due to its parameterizations, the transition region is smoothed out based on that of FO, the pressure also monotonically increases during the process.

The ratios  $\epsilon/T^4$  and  $3p/T^4$  are plotted as a function of temperature  $T$  for all the EoS in Fig.3. At zero baryon density, due to its fit to the lattice QCD results, only the LQCD gives correct asymptotic behaviour at high temperature. In this region, all the other EoS converge to the non-interacting ideal gas limit. On the other hand, in the low temperature limit, all the EoS approach the HRG model. The differences between CEP, FO and FOS come from the transition region around  $T \sim 160$  MeV. Since a first order phase transition of one-component system occurs at a constant temperature, it gives a vertical line in the case of FO. CEP is smoother in comparison with FO due to its phenomenological parameterization. Although the strangeness chemical potential is considered in FOS, it gives exactly the same result as FO. This can be understood by studying the intersection between the phase boundaries and x-axis in the bottom plot of Fig.1. Since

the two phase boundary curves coincide at zero baryon density, the choice between FO and FOS does not make any difference. The right panel in Fig.3 shows the results of CEP, FO and FOS for finite chemical potential (hence finite baryon density). The curves at zero chemical potential are also plotted for comparison purposes. It can be seen that  $\mu_B = 0.5$  GeV, which is beyond the critical point in the case of CEP, results a phase transition of the first order, therefore CEP behaves similarly to FO in this case. On the other hand, FOS is slightly different from them since the corresponding transition is not isothermal at finite baryon density. Nevertheless, all three EoS show very similar features in high and low temperature limits.

### III. NUMERICAL RESULTS AND DISCUSSIONS

Here we present results for the spectrum and flow parameter  $v_2$  using the three EoS discussed above as input into the hydrodynamical model NEXSPHERIO. The same initial conditions and freeze-out criterion are used in all cases.

For illustrating the hydrodynamical evolution, density plots for the energy density and entropy density are shown in Figs. 4 to 5. In Fig. 4 the energy density for a selected random fluctuating event is shown. The temporal evolution of the energy density in the transverse plane is calculated considering  $\eta = 0$  for three EoSs. In literature, usually smoothed IC is adopted which can be obtained in our case by averaging over different fluctuating IC of the same centrality window. Since it is understood that event by event fluctuating IC leads to important effects on elliptic flow [40, 41], triangular flow and two particle correlations [48, 49], the calculations in this work are done using such fluctuating IC. In the ideal hydrodynamic scenario, the total entropy of the system is conserved. To see the above results more quantitatively, the frozen-out entropy for the same event shown in Fig. 4 is considered at typical time instants and the results are depicted in Fig. 5. Due to the differences in EoS, the same IC may give different total entropy, so we plot entropy in percentage instead of using the absolute value.

It can be inferred from the plots that, at both  $\sqrt{s} = 130$  MeV and 200 MeV, the freeze-out process of LQCD stands out from other EoSs. This can be understood using Fig. 3, where the derivative of pressure with respect to temperature for LQCD is quite different from those of CEP, FO and FOS. In particular, for FO with a first order phase transition, the pressure remains unchanged during the transition process while the system continuously expands. In the case of CEP and FOS, the phase transition is smooth. However, in comparison to LQCD, the differences are not large. At 200 GeV, one observes that for LQCD it takes relatively less time for the system to freeze-out than the other three EoSs. This is probably due to its bigger derivative of the pressure

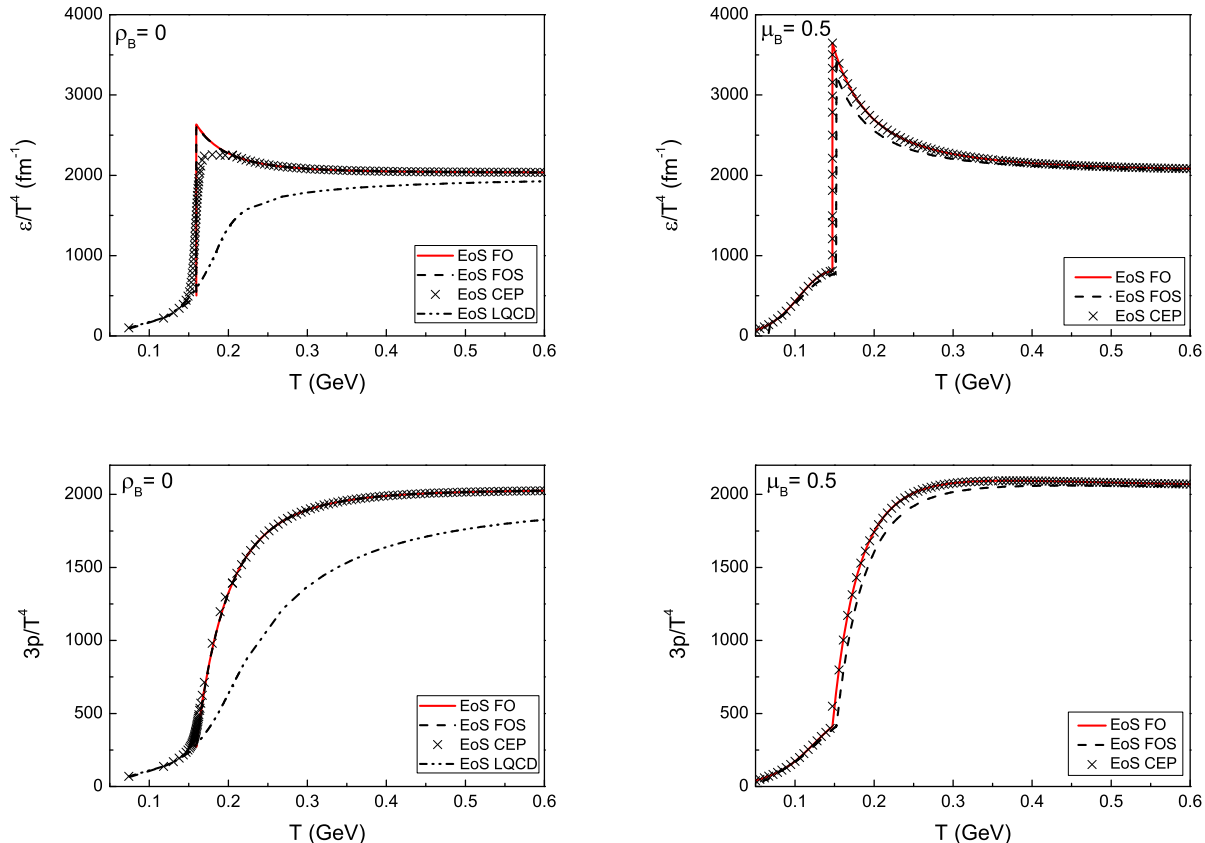


FIG. 3. (Color online)  $\epsilon/T^4$  and  $3p/T^4$  vs. temperature at zero baryon density (l.h.s.) as well as finite chemical baryon potential (r.h.s.) for EoS CEP, FO and FOS.

vs. temperature curve in the high temperature region. As can be seen in Fig. 3, on the other hand, the differences between CEP, FO and FOS are very small at high temperature limit. At 130 GeV, since the incident energy is smaller, the initial temperature is lower, and the local baryon density becomes slightly bigger. Therefore the properties of EoSs at finite baryon density and at the phase transition region play an increasingly important role. Consequently, the differences between FO, FOS and CEP become observable.

Next, particle spectra and elliptic flow are evaluated using 4000 NeXuS events for each centrality window at both 130 and 200 GeV Au-Au collisions. Balancing between a good statistics and efficiency, only 200 events are used for the calculation of particle spectra, but all 4000 events are used to evaluate the elliptic flow coefficients. At the end of each event, Monte-Carlo generator is invoked 100 times for decoupling. There are two free parameters in the present simulation, namely, an overall normalization factor to reproduce correctly the multiplicity and the thermal freeze-out temperature which is adjusted to the slope of transverse momentum spectra.

The results of the hydrodynamic simulations for the spectra and the flow parameters are shown in Figs. 6 to

10. Results for the  $p_T$  spectra are shown for all charged particles in Fig. 6. At a given energy, the same normalization is adopted for all different EoSs to evaluate the  $dN/d\eta$  yields. Our results are compared with PHOBOS' Au+Au data at 130 GeV [50] and 200 GeV [51]. For collisions at 130 GeV, a pseudo-rapidity interval  $-1 < \eta < 1$  is used in the calculations of the  $p_T$  spectra, which is then compared with the STAR data, where the pseudo-rapidity intervals are  $-0.5 < \eta < 0.5$  [52] and  $0.5 < |\eta| < 1$  [53] respectively. The freeze-out temperatures are determined as a function of centrality to fit the slope of the spectra, as shown in Table I.

For Au+Au collisions at 200 GeV, the pseudo-rapidity interval used in the calculations of  $p_T$  spectra is  $0.2 < y < 1.4$ , which is the same as that in the data [54]. Again, the freeze-out temperatures are determined as a function of centrality, which is shown in Table II. The same set of parameters for the freeze-out temperatures and renormalization factor was used for the different EoSs. It turned out that all three EoSs reproduce the measured  $\eta$  (not shown in the figures) and  $p_T$  spectra reasonably well, although some deviations occur at  $p_T > 3$  GeV for peripheral centrality windows.

Our results indicate that particle spectra are not very

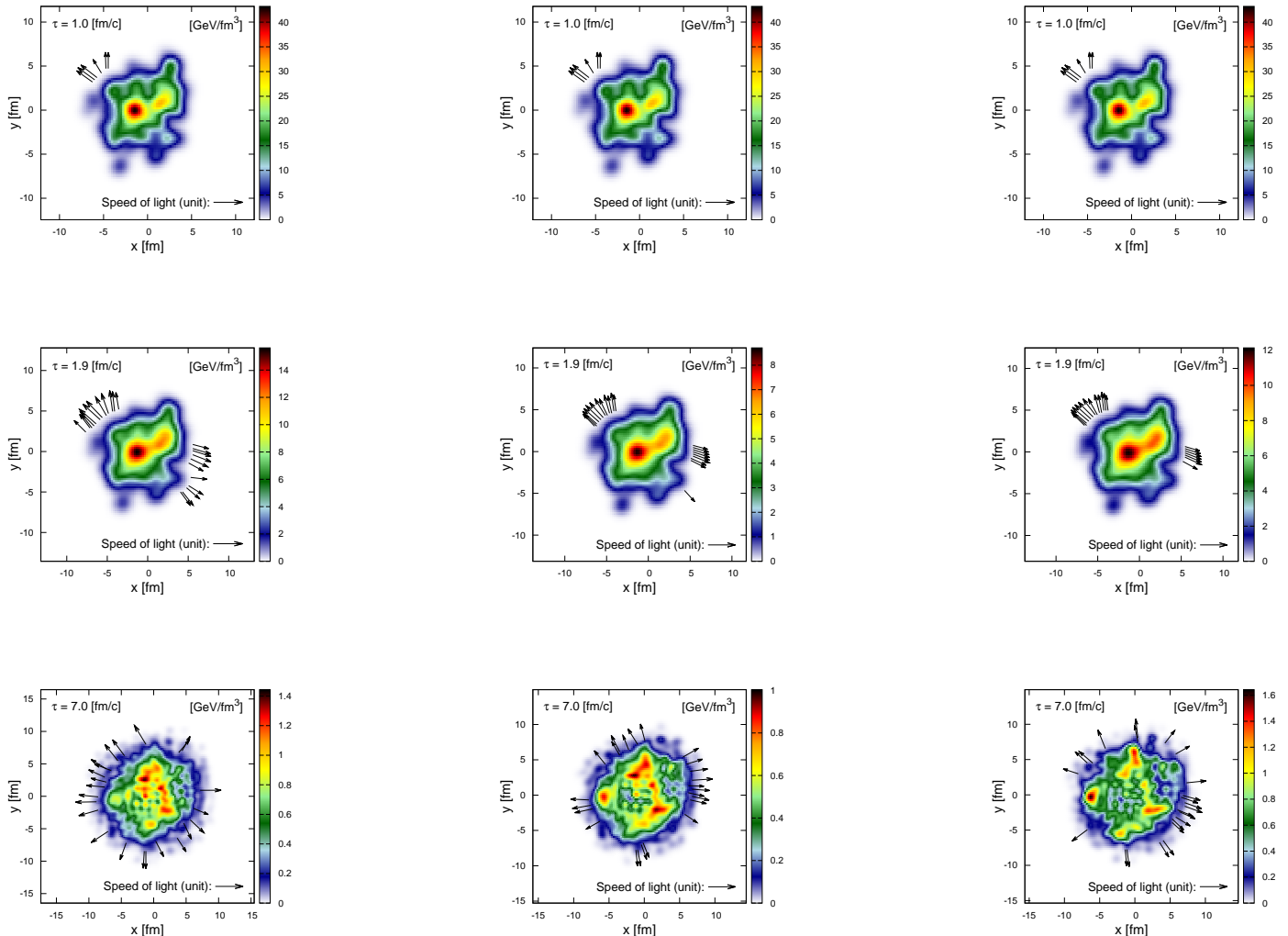


FIG. 4. (Color online) Temporal evolution of the energy density profile on the transverse plane  $\eta = 0$  for a given fluctuating event at 200 GeV using different EoS. The arrows show the velocities of the fluid elements on the freeze-out surface. Left: LQCD; Middle: CEP; Right: FOS.

Centrality (%)		Freeze-out temperature (MeV)
1	0 - 5	128
2	5 - 10	129.63
3	10 - 20	132.07
4	20 - 30	135.33
5	30 - 40	138.59
6	40 - 60	143.48
7	60 - 80	128

TABLE I. Centrality (%) vs. freeze-out temperature for Au+Au at 130 GeV.

Centrality (%)		Freeze-out Temperature (MeV)
1	0 - 6	128.16
2	6 - 15	130.44
3	15 - 25	133.70
4	25 - 35	136.96
5	35 - 45	140.22
6	45 - 55	143.48

TABLE II. Centrality (%) vs. freeze-out temperature for Au+Au at 200 GeV.

sensitive to the choice of EoS. This is consistent with conclusions obtained previously by using smoothed IC [12].

Next, we present the results for the elliptic flow parameter  $v_2$ . Here all the calculations are done by using the event plane method, and the results for  $v_2$  are presented

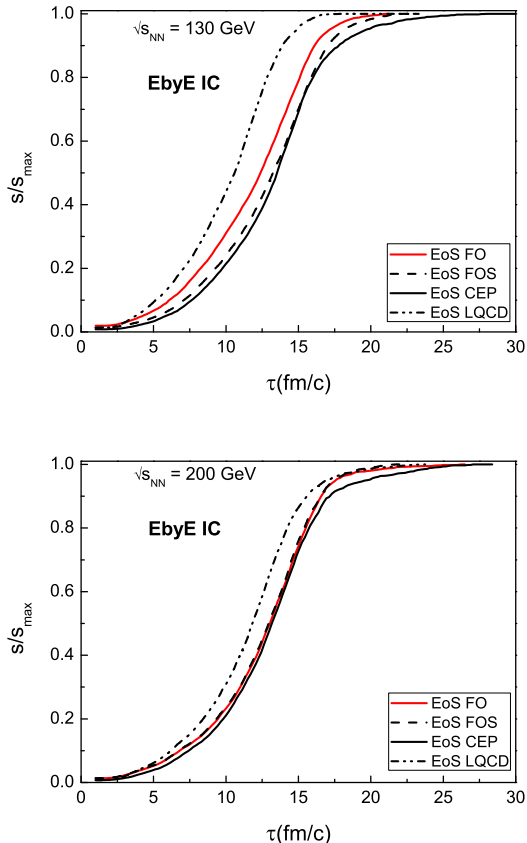


FIG. 5. (Color online) Freeze-out entropy as a function of evolution time for different EoS, the entropy is presented in percentage of its initial value. Top: A given fluctuating event at energy 200 GeV; Bottom: A given fluctuating event at energy 130 GeV.

as a function of pseudo-rapidity as well as of transverse momentum. For Au+Au collisions at 130 GeV, the calculated  $v_2$  as function of  $p_T$  is shown in the top plot of Fig. 7 and the data points are from the STAR collaboration [55]. In the top plot of Fig. 8, we present  $v_2$  as function of  $\eta$ ; data points are from the PHOBOS collaboration [56]. When calculating  $v_2$  as function of  $p_T$ , a cut in pseudo-rapidity  $|\eta| < 1.3$  was implemented. There is no momentum cut in the calculations of  $v_2$  as function of  $\eta$ . In both cases, the freeze-out temperature is taken to be  $T_f = 135.3$  MeV. Similar calculations of Au+Au collisions are carried out at 200 GeV, whose results are presented in the bottom panels of Figs. 7 and 8. In the calculations of  $v_2$  as function of  $p_T$  at 200 GeV, only particles in the interval  $0 < \eta < 1.5$  are considered, in accordance with the data of the PHOBOS collaboration [57]. The freeze-out temperature for this case is also taken to be  $T_f = 135.3$  MeV.

The calculations are also carried out for identified particles. In the left column of Fig.9, the results are shown

for  $v_2$  vs.  $p_T$  for identified particles at 130 GeV. The calculations were performed for 0 - 50% centrality window, where the experimental data are from the STAR collaboration [58, 59]. In the right column, we present the corresponding results of  $v_2$  vs.  $p_T$  for identified particles at 200 GeV. The calculations were done for 0 - 50% centrality windows, which are compared to the STAR data for 0 - 80% [60] and 0 - 70% [61].

From these plots, it is clearly seen that at small  $p_T$  the measured elliptic flow coefficients can be reasonably well reproduced by using all three EoSs. In fact, different EoSs give roughly similar results, and all of them fail to describe the data when  $p_T$  increases beyond  $\sim 2$  GeV due to the ideal hydrodynamics employed in this study. In order to discriminate the EoSs, we presented the results from different EoSs on the same plot and focus only in the low  $p_T$  region, as shown in Fig. 10. The upper-left plot of Fig. 10 shows the results of  $v_2$  vs.  $p_T$  for all charged particles at 130 GeV; the upper-right plot gives those at 200 GeV; the lower-left and lower-right plots present results at 200 GeV of 0 - 5% centrality of all charged particles and of identified pions, respectively. The data are from the STAR collaboration [61]. It can be seen that the results of LQCD are slightly different from those of CEP and FOS for  $p_T < 1$  GeV. The obtained  $v_2$  is slightly bigger, and describes better the data. This can be understood as follows. For an EoS featuring a first order phase transition, such as FO, the pressure gradient vanishes when the system enters this region. In the present case, although CEP and FOS describe smooth phase transitions, their properties are more similar to that of FO than to those of LQCD. For LQCD, it could be inferred from Fig. 3 that the pressure gradient is bigger than those from other EoSs in the high temperature region ( $T \geq 0.3$  GeV). As a result, in the case of LQCD, the initial spatial eccentricity of the system would be transformed into momentum anisotropy with the biggest amplified magnitude at high temperature as well as during the hadronization process. At 200 GeV, on one hand, the evolution of the matter spend more time in the QGP phase where most eccentricity is developed, therefore the asymptotic behaviour of LQCD at high temperature plays an increasingly important role, which makes it distinct from all other EoSs. On the other hand, at a lower incident energy, 130 GeV, the system develops relatively more anisotropy in the transition region, therefore the properties of the phase transition become more important. This makes the curve of CEP to become closer to that of LQCD.

On the basis of the results, one concludes that the observed differences due to different EoSs are generally small in size. Very recently, LQCD was extended to consider finite chemical potential [62] where the pressure is expanded in terms of chemical potentials by an Taylor expansion coefficients which are parameterized and compared to those obtained from lattice simulations. The effect of this novel version of LQCD is unknown, but not expected to be very big. Other factors, such as differ-

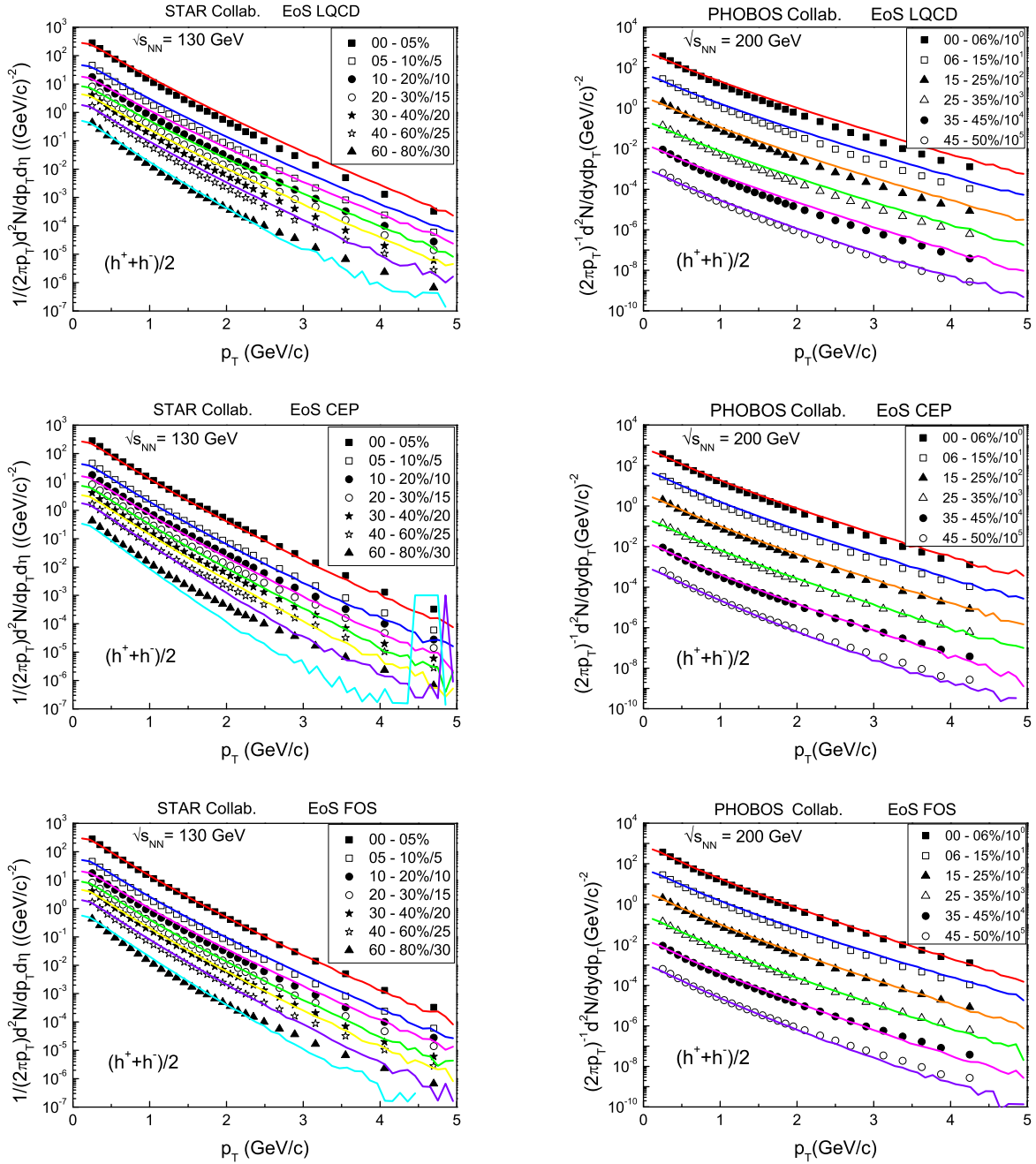


FIG. 6. (Color online)  $p_T$  spectra of all charged particles for Au+Au collisions at 130 GeV (left column) and 200 GeV (right column) for different EoS.

ent types of IC, fluctuations in the IC, viscosity, etc., should also be considered carefully. Generally, LQCD reproduces results closer to the data than the other EoSs investigated here. The EoSs with finite baryon/strangeness density also provide results with observable differences from those EoSs that do not impose conserved charges. Additionally, the time evolution, as well as momentum anisotropy, are shown to be affected. Therefore, it is interesting to introduce an EoS which considers finite chemical

potential while reproduces the lattice data at high temperature and zero baryon density region. Such an EoS may be employed to consistently study physical systems over a large range of densities and temperatures.

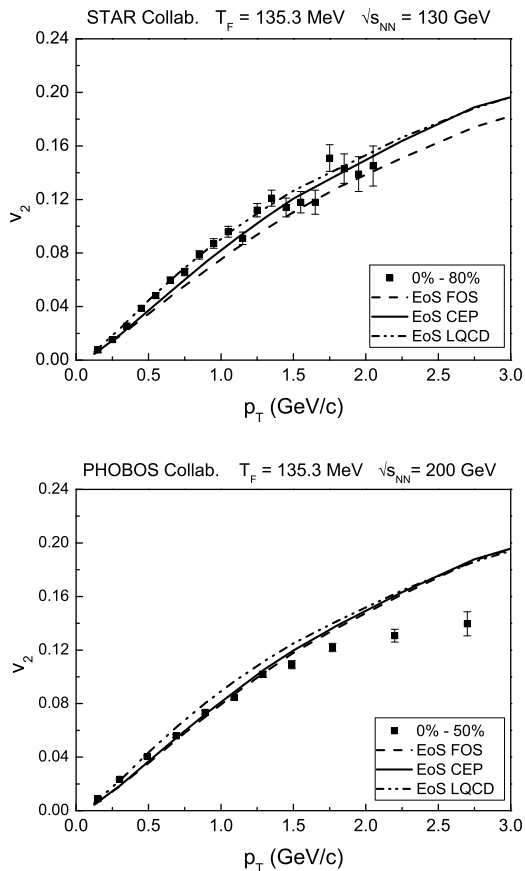


FIG. 7.  $v_2$  vs.  $p_T$  for all charged particles by using different EoS at 130 GeV for 0 - 80% centrality window (l.h.s.), and at 200 GeV for 0 - 50% centrality window (r.h.s.).

#### IV. CONCLUSIONS AND PERSPECTIVES

A systematic study on the role of EoS on hydrodynamical evolution of the system is carried out and discussed here. By adopting the same set of parameters, which consists of an overall renormalization factor and freeze-out temperatures, the particle spectra and elliptic flow coefficients are calculated by NEXSPheRIO code. The calculations cover a wide range of centrality windows at two different RHIC energies. It is found that all EoS successfully reproduce the particle spectra and elliptic flow at small  $p_T$  region. The hydrodynamical evolution of the system is affected by the EoS, which consequently leads to some small differences observed in elliptic flow.

#### V. ACKNOWLEDGMENTS

The authors are thankful for valuable discussions with Wojciech Florkowski and Tamás Csörgö. We gratefully acknowledge the financial support from Fundação de Amparo à Pesquisa do Estado de São Paulo (FAPESP),

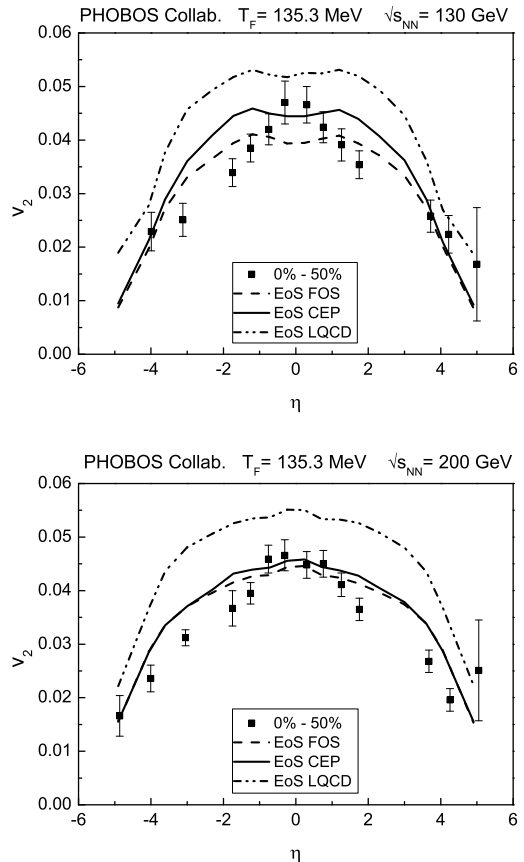


FIG. 8.  $v_2$  vs.  $\eta$  for all charged particles by using different EoS at 130 GeV at 0 - 50% centrality window (l.h.s.), and at 200 GeV (r.h.s.).

Fundação de Amparo à Pesquisa do Estado de Minas Gerais (FAPEMIG), Conselho Nacional de Desenvolvimento Científico e Tecnológico (CNPq), and Coordenação de Aperfeiçoamento de Pessoal de Nível Superior (CAPES).

[1] P. F. Kolb and U. W. Heinz, (2003), arXiv:nucl-th/0305084.  
 [2] E. Shuryak, Prog.Part.Nucl.Phys. **53**, 273 (2004), arXiv:hep-ph/0312227.

[3] U. W. Heinz and R. Snellings, Annu. Rev. Nucl. Part. Sci. **63**, 123 (2013), arXiv:1301.2826.  
 [4] C. Gale, S. Jeon, and B. Schenke, Int.J.Mod.Phys. **A28**, 1340011 (2013), arXiv:1301.5893.

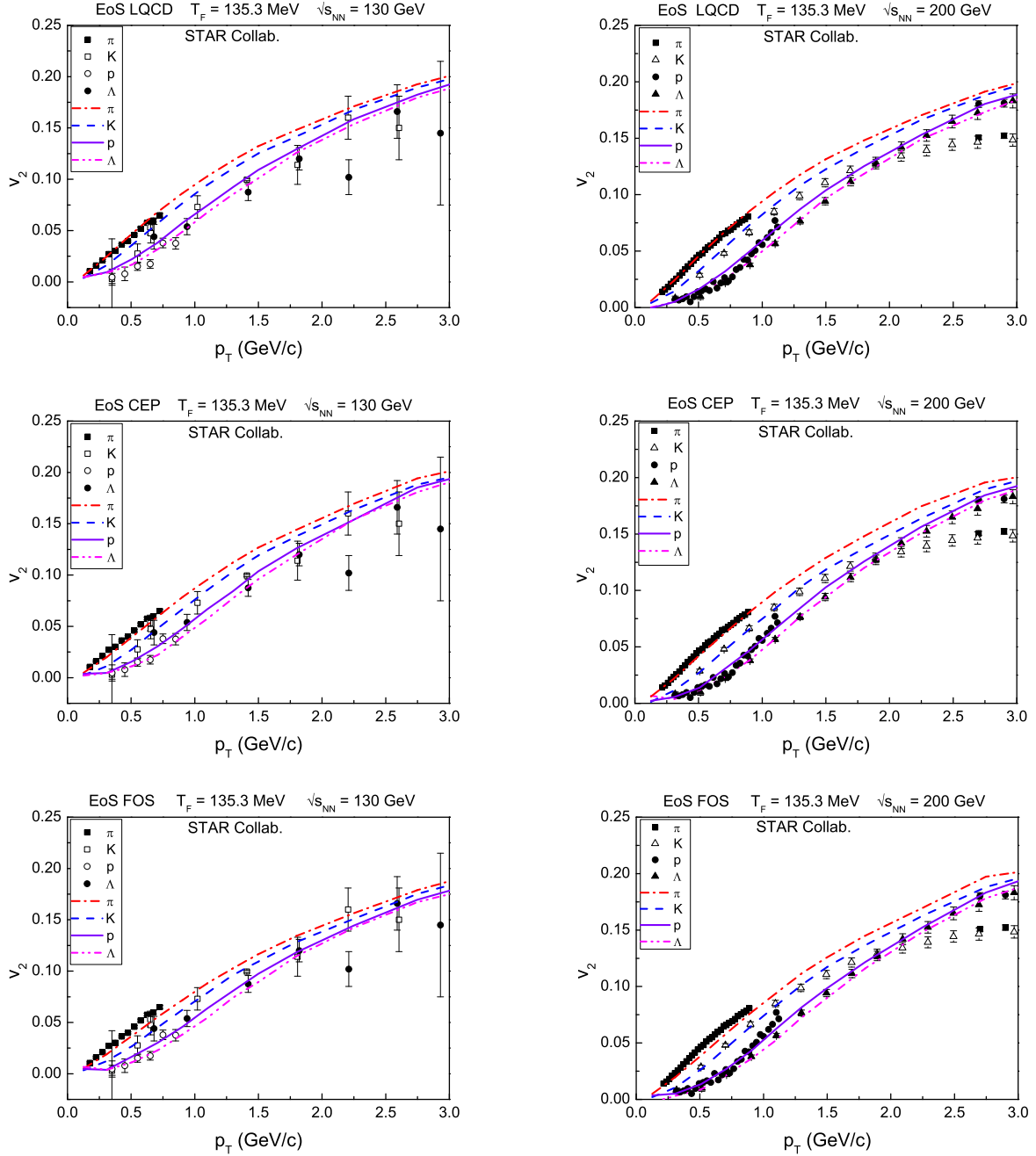


FIG. 9. (Color online)  $v_2$  vs.  $p_T$  for identified particles ( $\pi$ ,  $\kappa$ ,  $p$  and  $\Lambda$ ) by using different EoS at 130 GeV (left column), and at 200 GeV (right column).

- [5] Z. Fodor and S. Katz, JHEP **0203**, 014 (2002), arXiv:hep-lat/0106002.
- [6] F. Karsch, Nucl.Phys. **A698**, 199 (2002), arXiv:hep-ph/0103314.
- [7] Y. Aoki, G. Endrodi, Z. Fodor, S. Katz, and K. Szabo, Nature **443**, 675 (2006), arXiv:hep-lat/0611014.
- [8] A. Bazavov *et al.*, Phys.Rev. **D80**, 014504 (2009), arXiv:0903.4379.
- [9] M. Laine and Y. Schroder, Phys.Rev. **D73**, 085009 (2006), arXiv:hep-ph/0603048.
- [10] P. Braun-Munzinger, K. Redlich, and J. Stachel, (2003), arXiv:nucl-th/0304013.
- [11] P. Huovinen, Nucl.Phys. **A761**, 296 (2005), arXiv:nucl-th/0505036.
- [12] P. Huovinen and P. Petreczky, Nucl.Phys. **A837**, 26 (2010), arXiv:0912.2541.
- [13] P. Huovinen and P. Petreczky, J.Phys. **G38**, 124103 (2011), arXiv:1106.6227.
- [14] M. Chojnacki and W. Florkowski, Acta Phys.Polon. **B38**, 3249 (2007), arXiv:nucl-th/0702030.

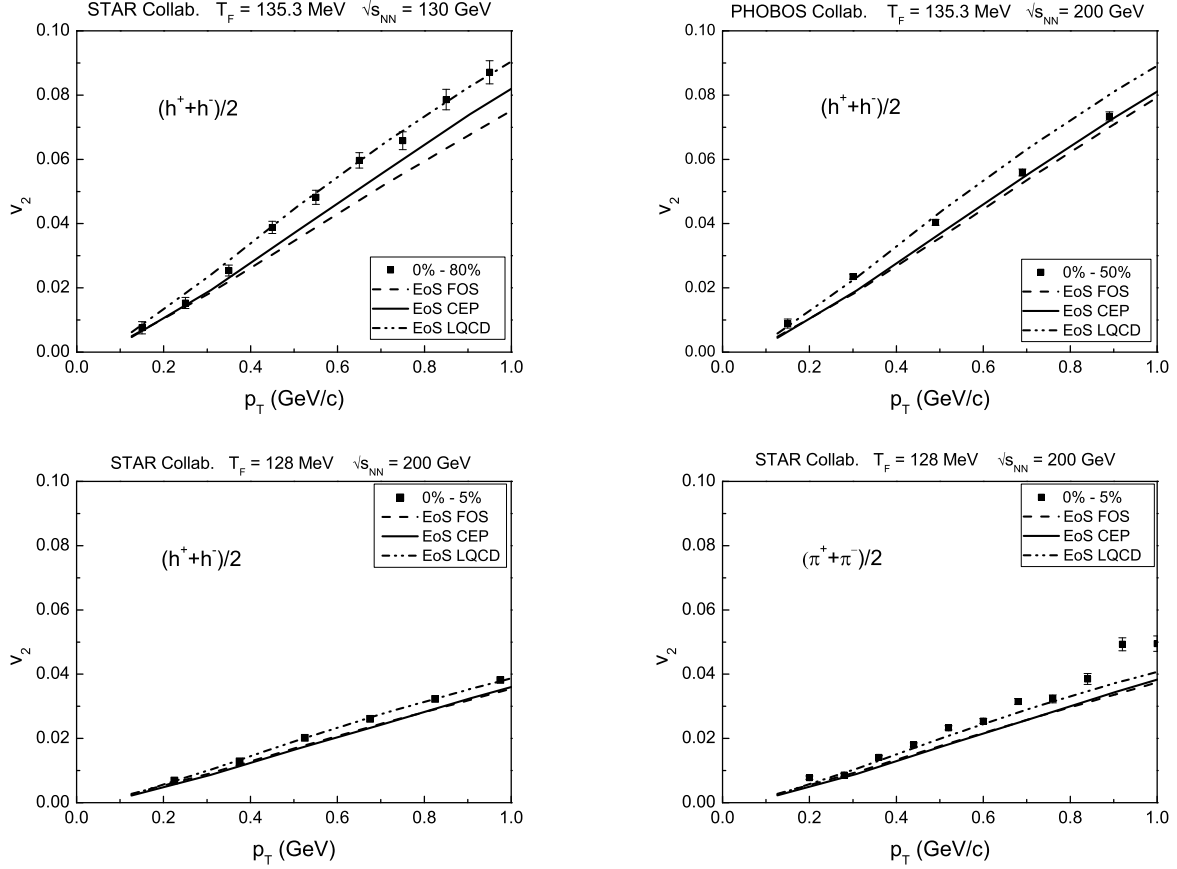


FIG. 10.  $v_2$  vs.  $p_T$  using different EoS. The upper-left plot is for all charged particle at 130 GeV of 0 - 80% centrality window; the upper-right plot is for all charged particles at 200 GeV of 0 -50% centrality window; the lower-left and lower-right plots present results at 200 GeV of 0 - 5% centrality window of all charged particles and of identified pions respectively.

- [15] M. Chojnacki, W. Florkowski, W. Broniowski, and A. Kisiel, Phys.Rev. **C78**, 014905 (2008), arXiv:0712.0947.
- [16] H. Song and U. W. Heinz, Phys.Rev. **C78**, 024902 (2008), arXiv:0805.1756.
- [17] T. S. Biro and J. Zimanyi, Phys.Lett. **B650**, 193 (2007), arXiv:hep-ph/0607079.
- [18] A. Chaudhuri, Phys.Lett. **B681**, 418 (2009), arXiv:0909.0391.
- [19] J. Steinheimer *et al.*, Phys.Rev. **C81**, 044913 (2010), arXiv:0905.3099.
- [20] Y. Hama, T. Kodama, and O. Socolowski Jr., Braz.J.Phys. **35**, 24 (2005), arXiv:hep-ph/0407264.
- [21] H. Muller and B. D. Serot, Phys.Rev. **C52**, 2072 (1995), arXiv:nucl-th/9505013.
- [22] W. L. Qian, R.-K. Su, and P. Wang, Phys.Lett. **B491**, 90 (2000), arXiv:nucl-th/0008057.
- [23] W. Qian, R.-K. Su, and H. Song, Phys.Lett. **B520**, 217 (2001), arXiv:nucl-th/0107036.
- [24] L. Yang, W. L. Qian, R.-K. Su, and H. Q. Song, Phys.Rev. **C70**, 045207 (2004), arXiv:nucl-th/0311017.
- [25] W. L. Qian, R.-K. Su, and H. Q. Song, J.Phys. **G30**, 1893 (2004), arXiv:nucl-th/0409063.
- [26] L. Yang, S. Y. Yin, W. L. Qian, and R.-k. Su, Phys.Rev. **C73**, 025203 (2006), arXiv:nucl-th/0506060.
- [27] A. Andronic, P. Braun-Munzinger, and J. Stachel, Nucl.Phys. **A772**, 167 (2006), arXiv:nucl-th/0511071.
- [28] ALICE Collaboration, B. Abelev *et al.*, Phys.Rev.Lett. **109**, 252301 (2012), arXiv:1208.1974.
- [29] V. Begun, M. I. Gorenstein, M. Hauer, V. Konchakovski, and O. Zozulya, Phys.Rev. **C74**, 044903 (2006), arXiv:nucl-th/0606036.
- [30] J. Fu, Phys.Lett. **B722**, 144 (2013).
- [31] Y. Hama *et al.*, Nucl.Phys. **A774**, 169 (2006), arXiv:hep-ph/0510096.
- [32] W. Broniowski, M. Chojnacki, W. Florkowski, and A. Kisiel, Phys.Rev.Lett. **101**, 022301 (2008), arXiv:0801.4361.
- [33] K. Fukushima, Phys.Lett. **B591**, 277 (2004), arXiv:hep-ph/0310121.
- [34] F. Karsch and E. Laermann, (2003), arXiv:hep-lat/0305025.
- [35] K. Dusling, G. D. Moore, and D. Teaney, Phys.Rev. **C81**, 034907 (2010), arXiv:0909.0754.
- [36] M. Luzum and J.-Y. Ollitrault, Phys.Rev. **C82**, 014906 (2010), arXiv:1004.2023.
- [37] H. Drescher, S. Ostapchenko, T. Pierog, and K. Werner, Phys.Rev. **C65**, 054902 (2002), arXiv:hep-ph/0011219.
- [38] H. Drescher, M. Hladik, S. Ostapchenko, T. Pierog, and K. Werner, Phys.Rept. **350**, 93 (2001), arXiv:hep-

- ph/0007198.
- [39] C. Aguiar, T. Kodama, T. Osada, and Y. Hama, *J.Phys.G* **G27**, 75 (2001), arXiv:hep-ph/0006239.
- [40] R. Andrade, F. Grassi, Y. Hama, T. Kodama, and O. Socolowski Jr., *Phys.Rev.Lett.* **97**, 202302 (2006), arXiv:nucl-th/0608067.
- [41] R. Andrade, F. Grassi, Y. Hama, T. Kodama, and W. Qian, *Phys.Rev.Lett.* **101**, 112301 (2008), arXiv:0805.0018.
- [42] W.-L. Qian *et al.*, *Int.J.Mod.Phys.* **E16**, 1877 (2007), arXiv:nucl-th/0703078.
- [43] O. Socolowski Jr., F. Grassi, Y. Hama, and T. Kodama, *Phys.Rev.Lett.* **93**, 182301 (2004), arXiv:hep-ph/0405181.
- [44] J. Takahashi *et al.*, *Phys.Rev.Lett.* **103**, 242301 (2009), arXiv:0902.4870.
- [45] W.-L. Qian, R. Andrade, F. Gardim, F. Grassi, and Y. Hama, *Phys.Rev.* **C87**, 014904 (2013), arXiv:1207.6415.
- [46] W.-L. Qian *et al.*, *J.Phys.G* **G41**, 015103 (2014), arXiv:1305.4673.
- [47] W.-L. Qian *et al.*, *Braz.J.Phys.* **37**, 767 (2007), arXiv:nucl-th/0612061.
- [48] B. Alver and G. Roland, *Phys.Rev.* **C81**, 054905 (2010), arXiv:1003.0194.
- [49] D. Teaney and L. Yan, *Phys.Rev.* **C83**, 064904 (2011), arXiv:1010.1876.
- [50] PHOBOS Collaboration, B. Back *et al.*, *Phys.Rev.Lett.* **87**, 102303 (2001), arXiv:nucl-ex/0106006.
- [51] PHOBOS Collaboration, B. Back *et al.*, *Braz. J. Phys* **34**, 829 (2004).
- [52] STAR Collaboration, C. Adler *et al.*, *Phys.Rev.Lett.* **89**, 202301 (2002), arXiv:nucl-ex/0206011.
- [53] STAR Collaboration, J. Adams *et al.*, *Phys.Rev.* **C70**, 044901 (2004), arXiv:nucl-ex/0404020.
- [54] PHOBOS Collaboration, B. Back *et al.*, *Phys.Lett.* **B578**, 297 (2004), arXiv:nucl-ex/0302015.
- [55] STAR Collaboration, K. Ackermann *et al.*, *Phys.Rev.Lett.* **86**, 402 (2001), arXiv:nucl-ex/0009011.
- [56] PHOBOS Collaboration, B. Back *et al.*, *Phys.Rev.Lett.* **89**, 222301 (2002), arXiv:nucl-ex/0205021.
- [57] PHOBOS Collaboration, B. Back *et al.*, *Phys.Rev.* **C72**, 051901 (2005), arXiv:nucl-ex/0407012.
- [58] STAR Collaboration, C. Adler *et al.*, *Phys.Rev.Lett.* **87**, 182301 (2001), arXiv:nucl-ex/0107003.
- [59] STAR Collaboration, C. Adler *et al.*, *Phys.Rev.Lett.* **89**, 132301 (2002), arXiv:hep-ex/0205072.
- [60] STAR Collaboration, B. Abelev *et al.*, *Phys.Rev.* **C77**, 054901 (2008), arXiv:0801.3466.
- [61] STAR Collaboration, J. Adams *et al.*, *Phys.Rev.* **C72**, 014904 (2005), arXiv:nucl-ex/0409033.
- [62] P. Huovinen, P. Petreczky, and C. Schmidt, (2014), 1407.8532.